CHAPTER IV

ELECTROSPUN POLYOXYMETHYLENE: SPINNING CONDITIONS AND ITS CONSEQUENT NANOPOROUS NANOFIBER **

Thontree Kongkhlang[1], Masaya Kotaki[2], Yasushi Kousaka[3], Toshikazu Umemura[3], Daigo Nakaya[4], and Suwabun Chirachanchai[1(*)]

[1]*The Petroleum and Petrochemical College, Chulalongkorn University, Soi Chula 12, Phyathai Road, Pathumwan, Bangkok, Thailand 10330.*

[2]*Advanced Fibro-science, Kyoto Institute of Technology, Matsugasaki, Sakyo-ku, Kyoto 606-8585, Japan.*

[3]*Mitsubishi Gas Chemical Company, Mitsubishi Building 5-2, Marunouchi 2-chome, Chiyoda-ku, Tokyo 100-8324, Japan.*

[4]*Thai Polyacetal Co., Ltd., Padaeng Industrial Estate, 1 Padaeng Road, Map-Ta-Phut, Rayong, Thailand 21150.*

***Corresponding author**

The present chapter is from the article published in *Macromolecules* **2008, 41, 4746–4752.

ABSTRACT

A successful electrospun polyoxymethylene (POM) nanofiber using a hexafluoroisopropanol (HFIP)-based solvent is reported. The nanofibers obtained show a significant nanoporous surface as a consequence of the spinning conditions, i.e. spinning voltage and relative humidity, as well as the polymer/solvent properties. The

oxyethylene unit in the polyoxymethylene copolymer decreases the nanofiber surface roughness and porosity, leading to a significant change in the specific surface area. A slight change in the molecular weight of the POM after electrospinning confirms that the nanofiber with nanoporous POM barely degrades or decomposes during the spinning. The electrospun POM nanofiber gives an inevitable nanoporous structure with high specific surface area (as much as 2 to 3 times higher) compared to those of the non-porous electrospun Nylon6 and porous electrsopun PAN reported in the past.

Keywords: polyoxymethylene, electrospinning, nanofiber, nanoporous

1. Introduction

Polyoxymethylene (POM) is a major engineering thermoplastic commonly used to replace metals and alloys because of its high tensile strength, impact resistance, stiffness, and good dimensional stability.[1] However, its low impact toughness, sensitivity to notch, and low heat resistance limit its range of applications. Changing the bulk plastic products to fine fibrous ones makes it possible for POM to be used for specific materials, such as for hydrocarbon fuel and hydraulic fluid filter membranes.

Melt spun POM is an alternative choice for exploring new applications; however, there is difficulty in how to prepare POM melt under elevated temperature conditions without degradation.[1] A copolymer of POM with an oxyethylene unit is one way to stabilize POM, since it shows less unzipping to retard the degradation.[2] For wet spinning, the primary concerns are the appropriate solvent to use and the spinning conditions.

Electrospinning is a unique wet spinning process to produce polymer fibers with diameters ranging from nano- to micro-scale.[3] The growth of research activities exploring the technology of electrospinning has occurred with various polymers (e.g. nylon 6[4], PLLA[5], PEO[6], and PE[7]), mostly from a polymer solution and some from

polymer melts. Most of the studies have focused on the generation of new nanostructured materials, on controlling the surface morphology, and on their applications. Some have also addressed the processing/property relationship in electrospun polymer fibers. The processing parameters included solution concentration and viscosity effects, accelerating voltage effects, spinning atmosphere effects, and the tip-to-target distance.[8,9]

As fine fibers provide high specific surface area, advanced applications are being proposed such as for enzyme or nanoparticle carriers in a controlled drug release system[10], scaffolds in tissue engineering[11], wound dressing mats[12], military wear with chemically and biologically resistant protection[13,14], nanofibrous membranes or filters[15], as well as for electronic sensors.[16,17]

To our knowledge, electrospun POM nanofiber has not yet been reported, which might be due to the difficulty in dissolving POM in general organic solvents and the ease of degradation. In order to explore the electrospinning of the POM nanofiber, all parameters—including solvent, polymer concentration, spinning voltage, fiber collecting conditions, and humidity—have to be considered. The present work, therefore, focuses on these parameters to achieve electrospun POM and its consequent nanofiber, which shows an inevitable nanoporous structure.

2. Experimental Section

Materials. A series of polyoxymethylene (POM) resins—i.e. POM homopolymer (POM0) and POM copolymers with oxyethylene units of 1.5 wt% (POM1.5), 4.4 wt% (POM4.4), and 13 wt% (POM13)— were provided by Mitsubishi Gas Chemical Company, Japan., Dimethylformamide (DMF, B_p~153°C, V_p at 20°C ~2.6 mmHg), 1,1,1,3,3,3-Hexafluoro-2-propanol (HFIP, B_p~58°C, V_p at 20°C ~120 mmHg) and toluene (B_p~111°C, V_p at 20°C ~22 mmHg) were purchased from Nacali Tesque, Inc., Japan. Glutaraldehyde (Glu, B_p~101°C, V_p at 20°C ~15 mmHg) was purchased from

Wako Pure Chemical Industries, Ltd., Japan. All chemicals were used without further purification.

Preparation of electrospun POM nanofibers. POM solutions with 3, 5, and 10 wt% in HFIP were prepared. The resulting clear and homogeneous solutions were electrospun with varied electrical voltages from 4–15 kV. The electrospun POM fibers were deposited onto a grounded sheet of aluminium foil, where the tip-to-collector distance was fixed at 10 cm and the volumetric flow rate was 0.5 mL/h. The spinning was done under a relative humidity of 55 and 75%. Each electrospun POM membrane was dried in a desiccator prior to use.

Characterizations. The surface morphology of the electrospun POM fiber was observed by a JSM-5200 JEOL scanning electron microscope. The average fiber diameter of each sample was determined using Image J software at 10,000×. The viscosity of the POM solution was determined using a DV-II+ viscometer (Brookfield) at 25°C using rotating speeds of 20 and 100 rpm. The weight-average molecular weight and molecular weight distribution were measured by a Tohso HLC-8220 gel permeation chromatograph (GPC) equipped with an RI detector and Tohso TSK-gel super H-RC and HM-N columns under an operating temperature of 40°C. An HFIP solution containing 10 mM CF_3CO_2Na was used as an eluent with a flow rate of 0.2 mL/min. Polymethyl methacrylate was used as the standard. Wide angle X-ray diffraction (WAXD) patterns were collected using a Rigaku RINT 2000 with CuK_α as the X-ray source, a scanning angle 2–50° 2θ, operating at 40 kV and 30 mA with a Ni filter. The crystallite size was estimated using the Scherrer equation, $\langle L \rangle_{100} = K\lambda/\beta\cos\theta$, where $\langle L \rangle_{100}$ is the crystallite size estimated from the (100) plane, K is the constant (0.9), λ is the wavelength of the X-ray (1.542 nm), β is the full width at half maximum peak intensity (FWHM), and θ is the Bragg angle. The FWHM or β was corrected for the peak broadening, which is caused by the diffractometer in which $\beta^2 = \beta^2_{obs} - \beta^2_m$, where β_{obs} is the measured peak width and β_m is the peak broadening due to the slit system. A Perkin Elmer Pyris Diamond DSC7 was used at a N_2 flow rate of 40 mL/min with a heating rate of 10°C/min from 25 to 200°C. The degree of crystallinity (χ_c) was estimated by assuming that the heat of melting per

unit mass of the crystalline material is identical to that of the melting of a 100% crystalline POM sample (i.e. 317.93 J/g, Iguchi *et al.*)[18]. The Brunauer–Emmett–Teller (BET) surface area was measured by using a surface area analyzer (SAA: Sorptomatic 1990, ThermoFinnigan Co., USA). The samples were degassed overnight in a vacuum at 100°C, and N_2 gas was used. A relative pressure range, P/P_0, of 0.05–0.3 was used for calculating the BET surface area.

3. Results and Discussion

The electrospinning process parameters—i.e. applied electrical voltage, needle-to-collector distance, solution feeding rate, and polymer solution parameters related to solubility, concentration, viscoelasticity, and solvent vapor pressure—are important for controlling fiber morphology.[8,19] In order to systematically study the variables of POM electrospinning, the working distance and the solution feed rate were kept constant at 10 cm and 0.5 mL/min, respectively.

Polymer jet formation. As the concentration, and the corresponding viscosity, is one of the most effective variables for controlling the fiber morphology,[20] the following investigations were conducted. The temperature was fixed at 40°C to avoid the precipitation of POM0 while the electrospinning solution was being prepared. At a concentration below 3 wt% (viscosity 50 mPa.s), electrospraying took place where the polymer jet broke into droplets and deposited on the target, resulting in a bead form. In contrast, due to the high viscosity of the solution at a concentration above 10 wt% (viscosity 800 mPa.s), the electrospinning was difficult to maintain, i.e. the droplet dried before a constant jet could be formed. As a result, the only possible concentration range for the spinning was ~ 3–10 wt%.

Fiber and surface morphology as an effect of polymer/solvent properties.

Solution concentration. Figure 4.1 shows the fiber morphology and frequency distribution of the fiber diameters of POM13 as a function of polymer concentration. The distribution of the fiber diameters shown in Figure 4.1 (d)–(f) was randomly measured from SEM photographs. Figure 4.1 (a)–(c) shows that the morphology of the fiber is drastically changed when the concentration of the polymer solution was varied. At 3 wt% concentration (Figure 4.1(a)), the electrospinning gives a bead-on-string fiber with bimodal distribution corresponding to the average fiber diameter of 250 nm and an average bead diameter of 2600 nm (Figure 4.1(d)). Continuous fibers without beads are obtained at the polymer concentration of 5–10 wt% (Figure 4.1 (b) and (c)). As the concentration increases, the average fiber diameter increases from 460 nm (Figure 4.1 (e)) to 700 nm (Figure 4.1(f)). Similar trends were also observed in the cases of POM0, POM1.5, and POM4.4 (see supporting information, Figure S1).

Copolymer content. Figure 4.2 is a series of SEM images of POM fibers with oxyethylene unit contents of 0, 1.5, 4.4, and 13 wt%, electrospun from 5 wt% HFIP solutions. It is clear that the oxyethylene unit content has a critical influence on pore formation. Fibers with a highly porous surface morphology were obtained in the cases of POM0, POM1.5, and POM4.4. When the oxyethylene unit content reaches 13wt% (POM13), the surface morphology of the electrospun fiber is drastically changed, where the highly porous morphology is reduced and only a trace amount of pores is observed on the surface of the fibers (Figure 4.2(d)). Bognitzki et al. proposed that the elongation of the pores along the fiber axis was the result of the uniaxial extension of the jet in an electric field.[5] The irregular porous fibers, or the complex rough surface (magnified micrographs in Figure 4.2 (a)–(c)), as well as the porous fibers with diameters of around 40–100 nm (magnified micrograph in Figure 4.2 (d)), implies the competition between the phase separation dynamics and the fast evaporation rate of HFIP during the electrospinning process. The average fiber diameters, shown in Table 4.1 were significantly reduced to half when the copolymer oxyethylene was increased to 13 wt%. In other words, the higher the oxyethylene unit content, the lower the average diameter.

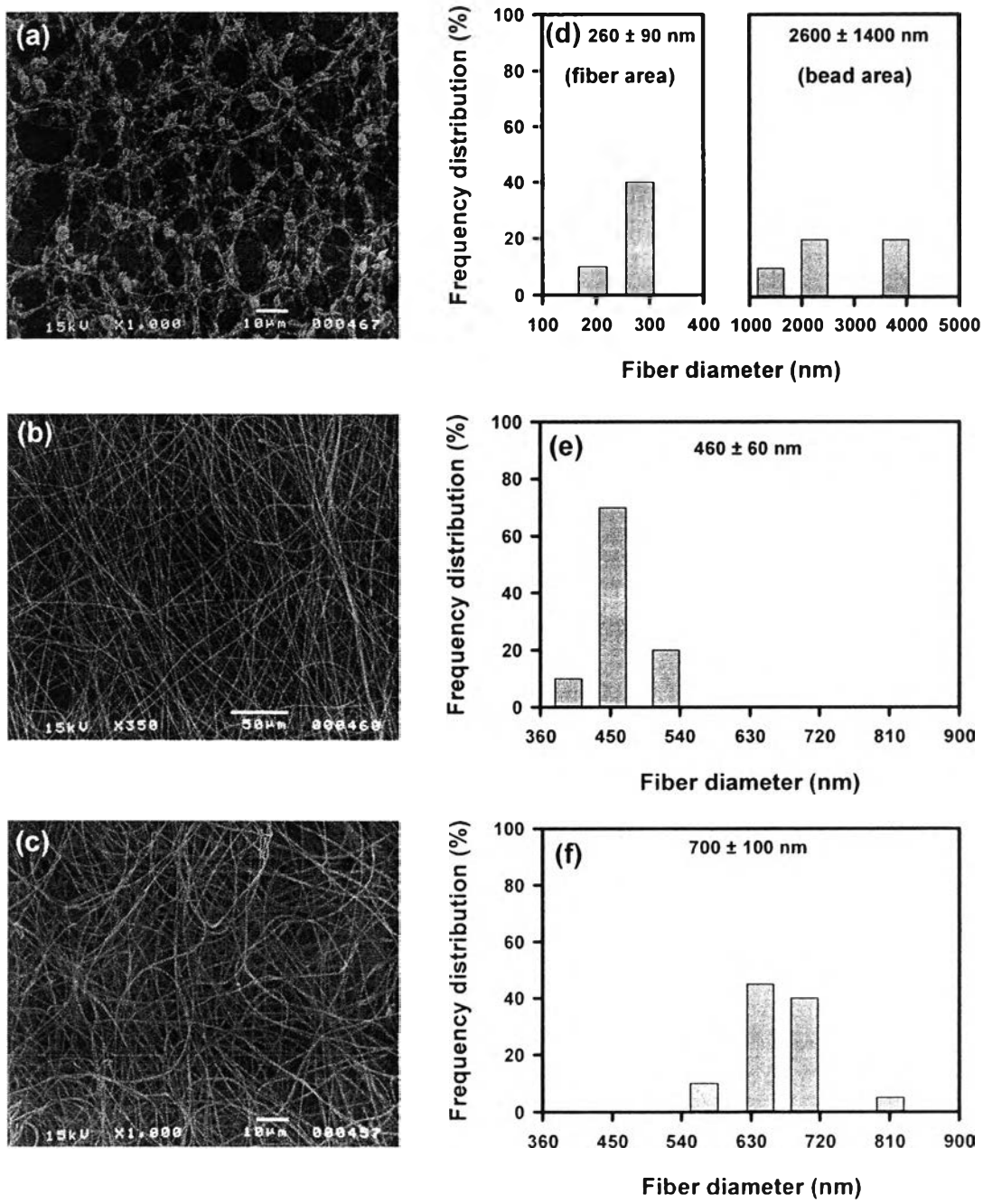

Figure 4.1. Scanning electron micrographs and frequency distributions of electrospun POM13 nanofibers as a function of polymer concentrations: (a) and (d) for 3 wt%; (b) and (e) for 5 wt%; and (c) and (f) for 10 wt%. (Electrostatic field strength = 15kV/10cm and relative humidity = 75%).

Doshi et al. concluded that the fiber diameter becomes smaller while it is being injected to the target due to (i) solvent evaporation and (ii) continuous stretching via the electrical force.[6] Here, we suspect that the number of oxyethylene units affects the elasticity of the polymer, leading to differences in stretching during the electrospinning. As a result, a rough surface (high porosity) and thick fibers (large fiber diameter) are observed with low oxyethylene content.

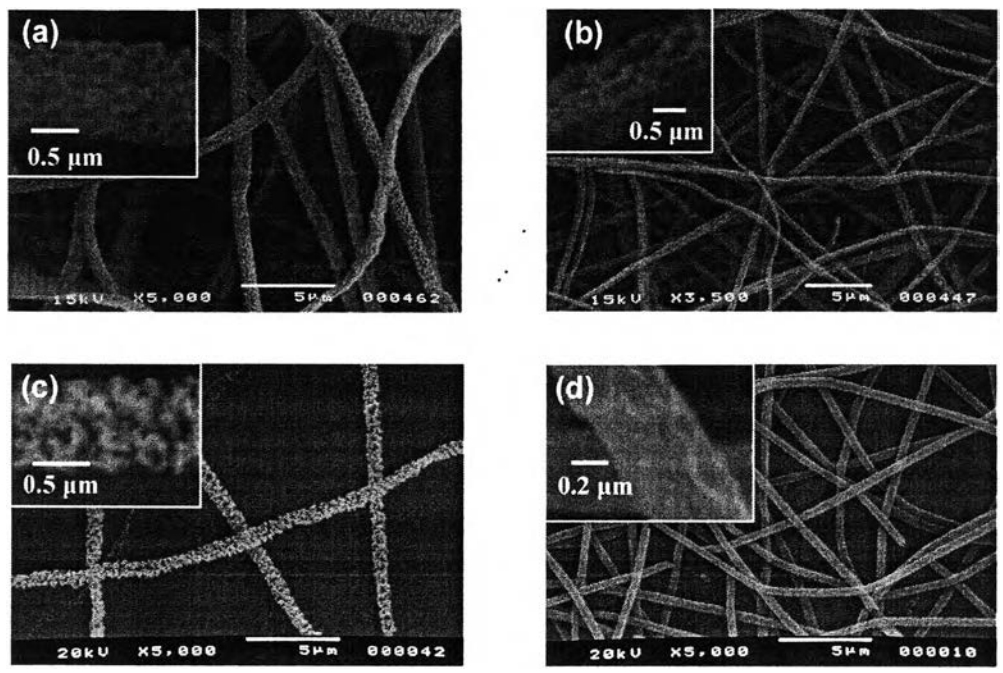

Figure 4.2. Scanning electron micrographs of the electrospun POM nanofibers from an HFIP solution with copolymer contents of (a) 0 wt%, (b) 1.5 wt%, (c) 4.4 wt%, and (d) 13 wt%. (Electrostatic field strength = 15kV/10cm and relative humidity =75%).

Table 4.1 Fiber diameter and specific surface area of electrospun POM nanofiber[a]

Sample	Diameter (nm)	Specific surface area (m^2/g)	Pore specific volume (cm^3/g)
POM0/HFIP	920 ± 160	23.73	0.15
POM1.5/HFIP	720 ± 200	34.92	0.97
POM4.4/HFIP	700 ± 120	57.04	0.15
POM13/HFIP	460 ± 70	15.06	0.04

[a] an electrostatic field strength = 15kV/10cm and relative humidity = 75%.

Solvent effects. The electrospinning of a polymer solution involves the rapid evaporation of the solvent while the jet stream is accelerated to the counter electrode.[5,6] The physical properties of the solvent play an important role in the process of pore formation. For comparison, therefore, a series of solvents with different boiling points (in other words, different vapor pressures) was used to prepare the POM solution. As only HFIP is a good solvent for POM, the volatility of the HFIP solution has to be adjusted by the mixing system of HFIP with lower vapor pressure solvents. Here, DMF, glutaraldehyde (Glu), and toluene were considered, at the level where the polymer solution is homogeneous with no precipitation. Mixtures of HFIP/DMF (94:6), HFIP/Glu (90:10), and HFIP/toluene (70:30) were used.

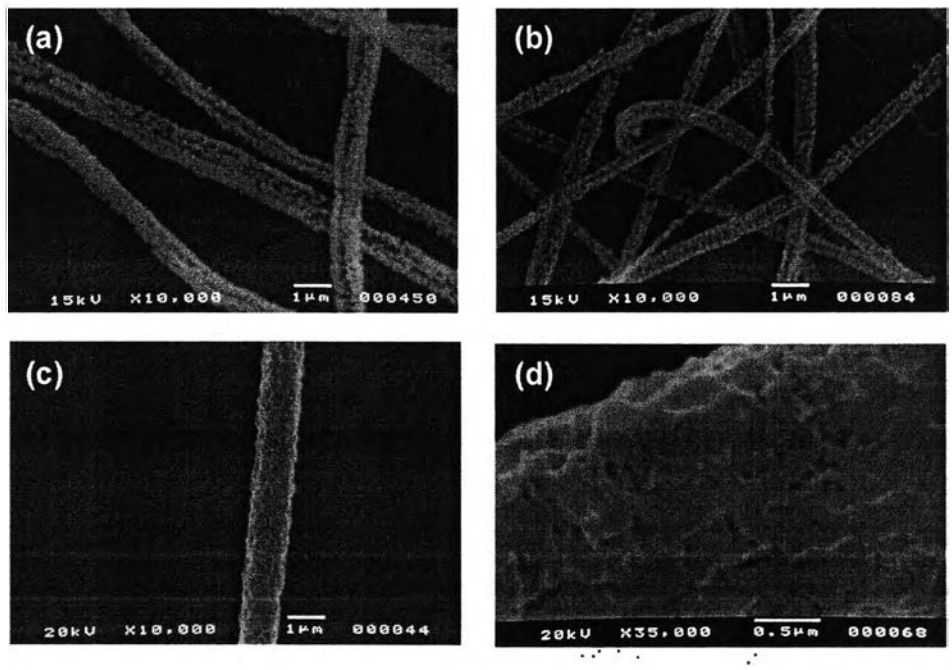

Figure 4.3. Scanning electron micrographs of the electrospun POM4.4 nanofiber from (a) HFIP/DMF (94:6), (b) HFIP/Glu (90:10), and (c) and (d) HFIP/Toluene (70:30) where (d) is magnified to observe the surface morphology of (c). (Electrostatic field = 15kV/10cm and relative humidity =75%).

The highly porous fiber of POM4.4 was chosen since it shows significant porosity when spun from the HFIP solution (Figure 4.2(c)). Figure 4.3 shows the effect of vapor pressure of the solvent mixture on the surface morphology. The fibers show high porosity with an average diameter of 1 μm in the case of HFIP/DMF (94:6). This implies that 6%DMF may not be sufficient to change the morphology. It should be noted that although the vapor pressure of DMF is the lowest, compared to Glu and toluene, its small amount, 6 wt%, was still not enough to retard the rapid evaporation rate of HFIP. Because a DMF amount over 6% initiated the precipitation of POM, the use of the DMF mixture was limited. Similar porous fibers were obtained in the case of HFIP/Glu (90:10), although a difference in fiber diameters was identified (Figure 4.3(b)). For

70:30 HFIP/toluene (Figure 4.3(c)), the porous density decreases significantly, as evidenced by the coarse surface morphology compared to those of the fibers from HFIP (Figure 4.2(c)) or other mixtures (Figure 4.3 (a) and (b)). This implies that 30% toluene effectively reduces the evaporation of HFIP, resulting in the change in surface morphology of the fiber. Figure 4.3 (d) clarifies the surface morphology with 35,000× magnification. It should be noted that the pores still exist, but they are rather regular with an average diameter as small as 40 nm. Although the solvents were varied, we found that the electrospun POM nanofiber inevitably formed a nanoporous structure.

Fiber and surface morphology as an effect of spinning conditions.

Spinning voltage. The voltage required to eject a charged polymer jet at the nozzle depends mainly on solution viscosity.[21] When the viscosity increases, the electrical forces required to overcome surface tension and viscoelastic force for fiber stretching has to be increased; as a result, an initial voltage, or so-called threshold voltage, is also increased. By keeping the polymer concentration constant at 5 wt%, the threshold voltage for the fine fiber without beads was 4kV. Figure 4.4 shows the SEM images and pore size distribution graphs of POM13 fibers when the voltage was varied from 4 to 15 kV. Here, the important information is that even though the voltage has been changed, the fibers obtained are inevitably nanoporous. Figure 4.4 shows an important point of two typical morphologies initiated by the spinning voltage, i.e. one is "regular pits" on the fiber surface, when the electrical voltage was 15 kV (Figure 4.4(d)), the other is connected and rough pores throughout the fiber, so called "pore-riddled fiber", when the electrical voltage was in the range of 4–10 kV (Figure 4.4 (a)–(c)). These fibers have an average pore size varying from the tens to the hundreds of nanometers (Figure 4.4 (e)–(g)). Figures 4.4 (d) and (h) show that in the case of the spinning voltage at 15 kV, the pits are shallow with an average diameter of about 30–100 nm and a length of about 150–200 nm with the long axis of the pits being stretched along the fiber axis. Considering the high vapor pressure of the HFIP solution, the higher the electrical voltage, the faster the rate of polymer ejection; hence, there is a

shorter evaporation time between the tip-to-target distance. This supports our speculation that the evaporation time of HFIP before the fiber reaches the target collector might be the key factor initiating a fine fiber with an inevitable porosity. It should be noted that the use of HFIP for the electrospinning of POM4.4 initiated the pore-riddled fiber in all ranges of applied voltages, i.e. 4–15kV (See supporting information, Figure S2).

The fiber diameter decreases from about 1 μm to 400 nm with an increase of spinning voltage up to 15 kV, or an increase of the corresponding electric field strength up to 1.5 kV/cm^{-1}, as shown in Figure 4.5. The dependence of the fiber diameter on the electric field strength leads to a power law relationship of fiber diameter $\sim(\text{Voltage})^{-0.67}$, indicating that the voltage plays an important role in determining the fiber diameter. An increase in the electrospinning voltage generally initiates an increase in mass flow rate from the capillary tip to the target collector when all other variables (conductivity, dielectric constant, and flow rate of solution to the capillary tip) are constant. Nevertheless, an increase of the applied voltage, i.e. an increase of the electric field strength, enhances electrostatic repulsive forces on the fluid jet, resulting in finer fiber formation. K. Gao also reported that an increase in voltage induces a decrease in fiber diameter in the case of electrospun PVDF fibers.[22]

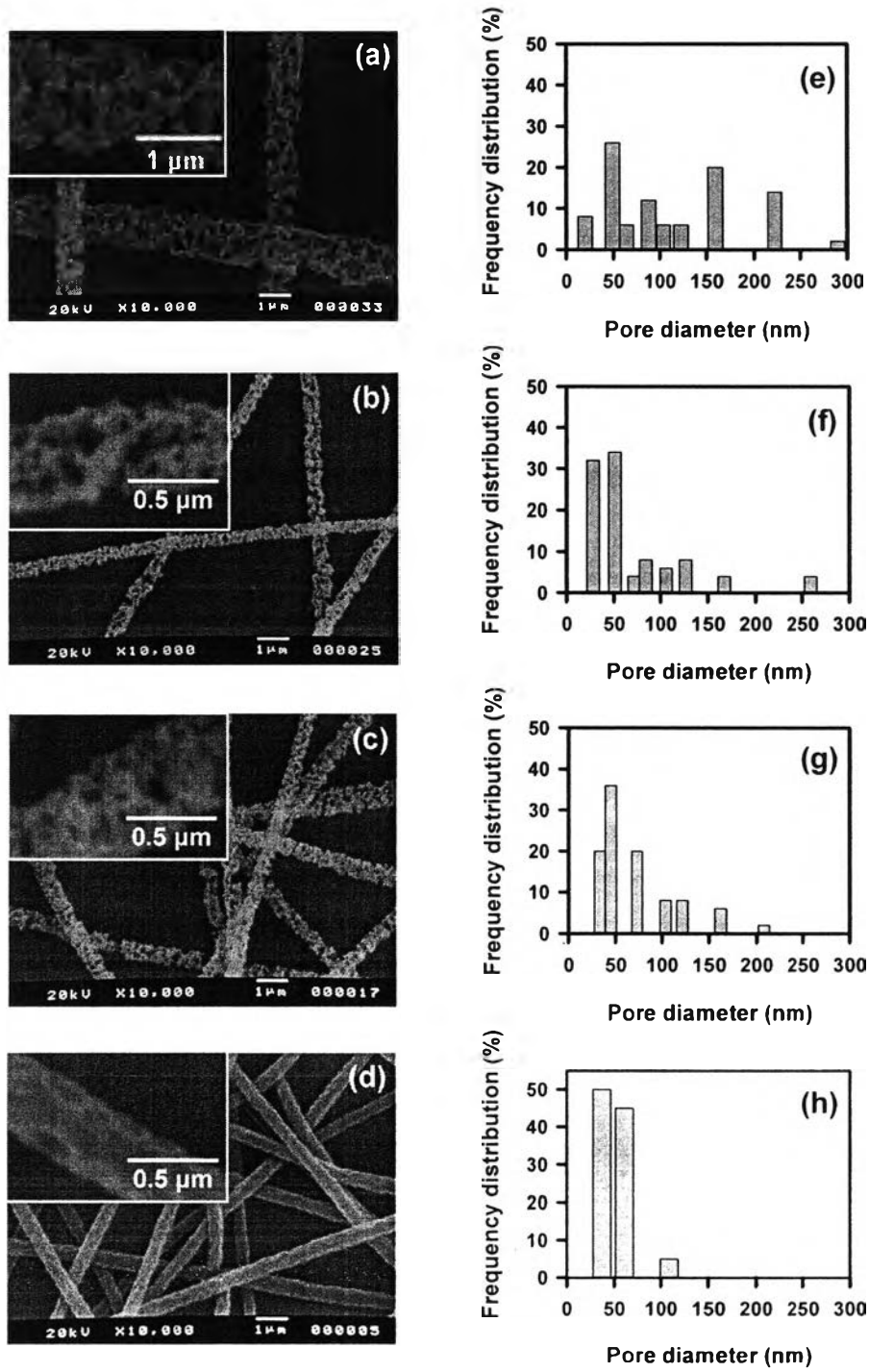

Figure 4.4. Scanning electron micrographs of the electrospun POM13 nanofibers from an HFIP solution at 75% relative humidity, and pore size distributions as a function of electrical voltages: (a) and (e) for 4kV; (b) and (f) for 6kV; (c) and (g) for 10kV; and (d) and (h) for 15kV. (Tip-to-target distance = 10 cm).

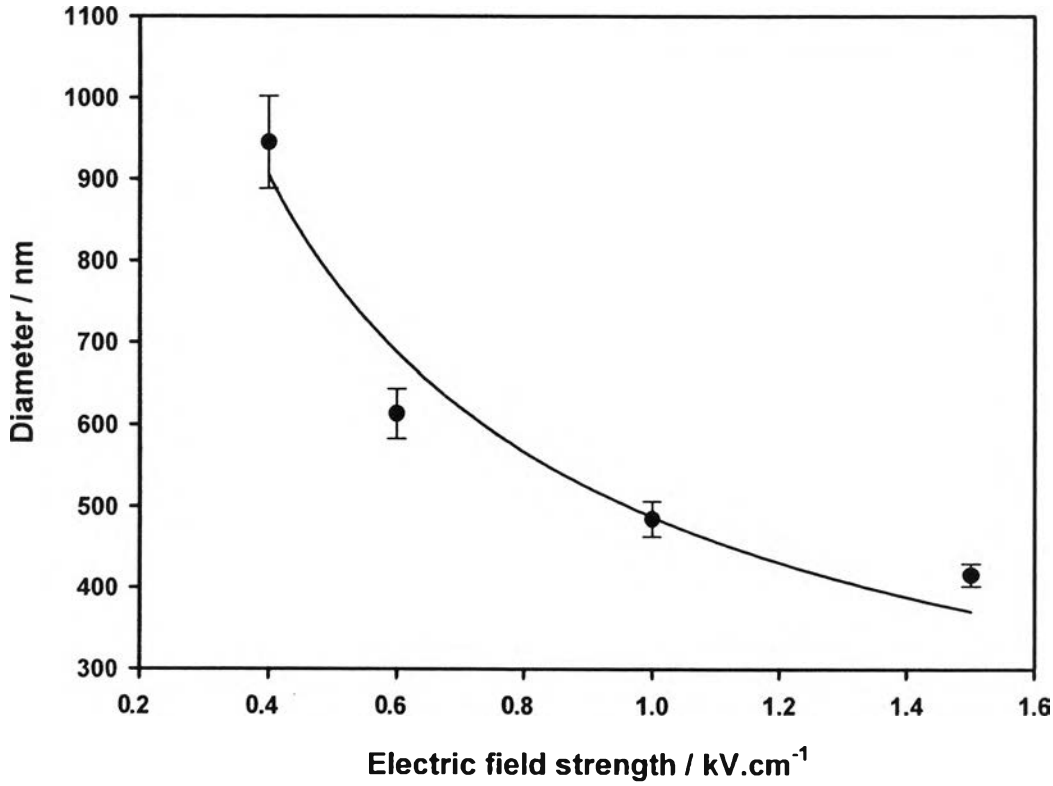

Figure 4.5. Fiber diameters as a function of electric field strength.

Relative humidity. It is important to note that humidity also plays an important role in controlling surface morphology. Casper et al. reported that electrospun PS/THF had a smooth surface until the relative humidity was above 31% (>31% RH). At either 50% or 70% RH, electrospun PS fibers gave regular pores without any differences, and those pores were observed only on the surface.[9]

In our case, however, 55% RH and 75% RH induced much different nanoporous structures. For example, when the voltage was maintained at 4–10 kV, but changing the relative humidity from 75% to 55%, the pore-riddled structure (Figure 4.4 (a)–(c)) gradually changed to the regular-pore structure (Figure 4.6(a)–(c)). The conditions shown in Figure 4.4 (c) and Figure 4.6 (c) are good cases to demonstrate how

the synergistic effects of electrical voltage and relative humidity drastically change the fiber morphology from pore-riddled to regular pores.

Relative humidity also influences the pore diameter and distribution. Comparing Figure 4.4 (e)–(g) with Figure 4.6 (e)–(g), it is clear that the pore diameters are decreased and the distribution becomes narrow, especially in the case of an applied voltage of 10 kV.

In the case of 15 kV, the differences in fiber porosity are not that significant. This might be due to the main effect of the applied voltage at 15 kV, which already initiated regular pores with rather smooth surfaces. However, the distribution becomes much smaller with a pore diameter of 20–60 nm when the % RH was reduced to 55 % (Figure 4.6 (h)).

It is important to point out that, for the reported electrospun PS, the humidity at 50 and 70% RH did not change the morphology of the nanofiber.[9] However, in our case, the %RH at this range initiated a significant change in fiber morphology, diameter, and distribution. Based on this result, a study on fiber morphology related to variation of the humidity is presently being carried out.

The cross-section of the nanofiber is another important point to discuss. For example, Megelski et al. observed a cross-section by TEM to find a ribbon shaped PS fiber with densely packed nanopores only on the surface.[8] In our case, we used POM13 as a representative case since it shows the most regular pitting compared to other POMs. The spinning voltage at 4 kV clearly shows nanopores throughout the fiber, as observed from the cross-section SEM micrograph (Figure 4.7(a)). Here, an attempt to overcome the nanoporosity by increasing the applied voltage (see *spinning voltage*) to 15 kV was considered. As shown in Figure 4.7 (b), the cross-section of the POM13 still shows a similar but less significant nanoporosity.

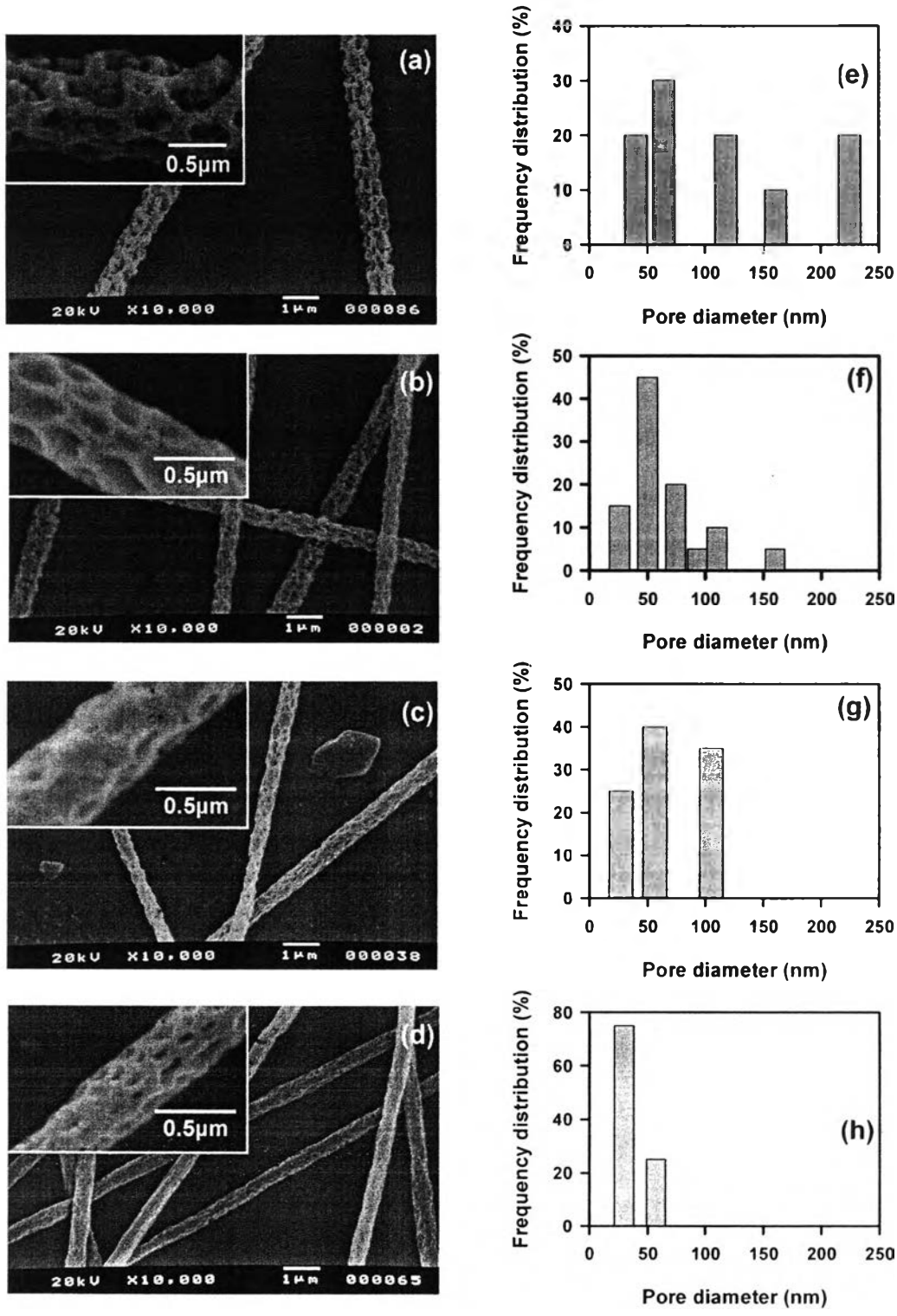

Figure 4.6. Scanning electron micrographs of the electrospun POM13 nanofibers from an HFIP solution at 55% relative humidity, and pore size distributions as a function of electrical voltages: (a) and (e) for 4kV; (b) and (f) for 6kV; (c) and (g) for 10kV; and (d) and (h) for 15kV. (Tip-to-target distance = 10 cm).

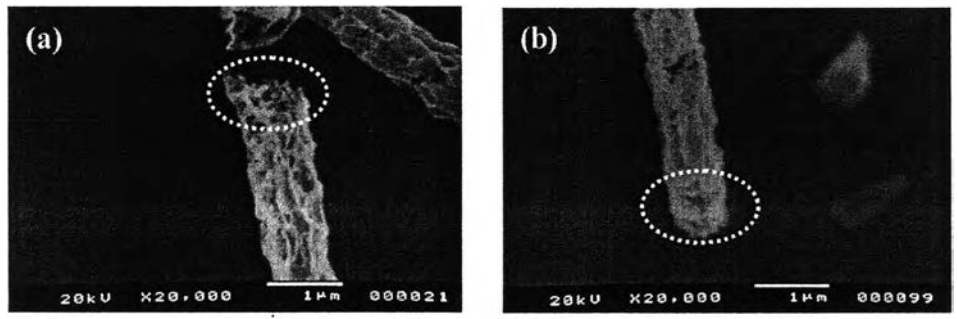

Figure 4.7. Scanning electron micrographs showing a cross-section of POM13 nanofibers from an HFIP solution at 55% relative humidity, electrospun at (a) 4 kV and (b) 15 kV. (Tip-to-target distance = 10 cm).

Pore formation of electrospun POM nanofiber. Srinivasarao et al. showed a beautiful three-dimensional ordered array of monodispersed air bubbles on PS thin film by allowing the moisture condensing on the cold surface to form water droplets during solvent evaporation under the breath figure mechanism.[23] For electrospun PS, Casper et al. reported that the electrospun PS fibers as a consequence of breath figure and phase separation mechanism were not like the ordered arrays of a uniformly shaped porous surface.[9]

In our case, although HFIP is a high vapor pressure solvent, the electrospun POM nanofibers show various pore sizes and shapes, suggesting that the mechanism might be based on phase separation. Van de Witte et al. reported that the phase separation mechanism involves (i) thermally induced phase separation (TIPS), (ii) vapor induced phase separation (VIPS), (iii) immersion precipitation, and (iv) air-casting of a polymer solution, which are under thermodynamic instability as the driving force.[24] Considering TIPS, as the HFIP is rapidly evaporated when the POM jet is being ejected, the lowering of temperature at the fiber surface is significant, resulting in phase separation. A reduction in the applied voltage further increases the possibility of the HFIP evaporating before reaching the target; as a result, pore-riddled fibers were

obtained at lower electric fields (4–10 kV) (Figure 4.4). This also supports TIPS. For VIPS, moisture plays an important role in the non-solvent content deposited on the fiber surface. This might be the reason why, when there is only a little % RH reduction, a drastic change from a pore-riddled fiber to regular pit on smooth fiber surface could be observed (Figures 4.4 and 4.6). The VIPS is also a factor related to the changes on the fiber surface when the second solvent (i.e. DMF, Glu, or toluene) is introduced into the HFIP. The addition of a second solvent not only reduces the evaporation rate of the HFIP but is also favorable or unfavorable for water dissolving in the solvent mixture. Water is soluble in DMF and Glu, making the system not significantly different from that of HFIP. In contrast, water barely dissolves in toluene; as a result, phase separation is prevented and a smooth surface with fewer pores, in the case of HFIP/toluene, could be observed (Figure 4.3 (d)).

Nucleation and growth (NG) and/or spinodal decomposition (SD) are also involved with the phase separation.[24] An interconnected pore structure is a characteristic of the NG, whereas a cellular pore structure is produced by the SD.[24,25] In our case, neither the interconnected pore structure nor the cellular pore structure was clearly distinguished. However, a small interconnected structure was recognized in the cross-section of the POM nanofiber (Figure 4.7). This implies that the porous structure initiated in the initial stage of the SD, due to the fast evaporation rate and crystallization rate. Considering the effect of solvent and taking the SD into consideration, the polymer-poor regions are apparently altered into pores, whereas the polymer-rich regions develop into the matrix. In this case, the spinodal decomposition might be stopped immediately, resulting in a co-continuous structure, because the solidification process is also very fast due to the high evaporation rate of the HFIP.

It should be noted here that although we suspect the pore is initiated based on the high evaporation rate of the HFIP, in the cases of Nylon 6[26,27] and Nylon 12,[26] the HFIP barely affected the fiber morphology. We suspect that the hydrogen bond network might compensate for the evaporation of the solvent molecule and recover the surface smoothness.

As mentioned above, although the pore formation is discussed based on all possible variables (such as solvents and their vapor pressure, electrical voltage, and moisture content) the type of POM is also a point requiring consideration. It should be noted that POM13 dissolves very well in HFIP, as compared to other POMs. This might cause the slow evaporation of HFIP due to the strong interaction of the POM13 polymeric chains and the HFIP molecules. Therefore, we suspect that an oxyethylene unit in the POM might retard the TIPS mechanism. At present, in order to determine how the oxyethylene unit in POM is involved with the VIPS mechanism, a series of electrospun POM nanofiber obtained from various solvent mixtures and under various humidity conditions are under investigation.

Specific properties of the electrospun POM fibers.

Stability. As the fiber obtained showed a significantly porous surface morphology, it is important to identify whether that porous morphology is the consequence of POM degradation or not—in other words, whether or not the electrospinning initiates the degradation. Table 4.2 shows a slight decrease in Mw (10–30%) for all POM types. In the case of POM13, the decrease in molecular weight is only about 10%. This implies that the POM degradation, if it happens, is not significant since the POM possibly maintains its structure during fiber spinning, and the porosity of the fiber might mainly come from the rapid solvent evaporation. The copolymer content may also help to prevent the degradation and as a result the smooth fiber surface is observed, as shown in Figure 4.2(d). It should be noted that electrospinning initiated the fiber alignment at the nanoscopic level.[28] This might compensate for the molecular weight reduction due to the slight degradation.

Another study on how the decrease in molecular weight affects the mechanical properties was carried out. An in-house electrospinning apparatus, with a rotating disc collector for fiber alignment, was used. At that time, if the degradation was initiated by electrospinning, the disc collector shear force would induce more degradation; as a result, the tensile strength should become lower. The aligned POM0/HFIP nanofiber was

collected using a disc linear velocity of 630m/min and 1890 m/min (4mm×40mm×0.07mm). It was found that the mechanical properties of the aligned nanofibers exhibited an increase in tensile strength (~300 MPa at 1890 m/min and ~70 MPa at 630 m/min)—see supporting information (Figure S3).

Table 4.2 Various properties of electrospun POM nanofibers[a] as compared to POM resin

Properties	POM resin with different oxyethylene unit				Electrospun POM nanofiber with different oxyethylene unit			
	POM0	POM1.5	POM4.4	POM13	POM0	POM1.5	POM4.4	POM13
M_w[b] (10^5, g/mol)	2.00	2.44	2.19	1.75	1.55	1.90	1.30	1.55
M_w/M_n[b]	2.40	2.55	1.78	2.05	2.80	3.05	3.33	2.35
Crystallinity (%)	-	-	70[c]	-	88	80	77	66
Crystallite size (Å)	-	-	117.6[c]	-	96.6	90.1	70.5	68.8
T_m (°C)	176	168	162	152	175	168	163	152
T_c (°C)	145	145	142	133	150	148	145	136
ΔH_m (1^{st} heating, J/g)	-	-	-	-	174	170	162	145
ΔH_m (2^{nd} heating, J/g)	168	157	143	137	168	160	149	125

[a] electrospun from HFIP solution with an electrostatic field strength of 15kV/10cm and relative humidity of 75%.

[b] measured by GPC with HFIP as an eluent.

[c] cast POM 4.4 in HFIP.

Crystallinity. It is important to note that the nanofiber formation possibly initiates the polymer chain alignment leading to changes in the packing structure and thermal properties. Crystallite size and degree of crystallinity, shown in Table 4.2, support this speculation. For the solution cast POM4.4 film, the degree of crystallinity is about 70% and the crystallite size is about 118Å. However, for the electrospun POM4.4 nanofiber from the HFIP solution, the degree of crystallinity increases to 77% and the crystallite size decreases to 70.5Å, implying the orientation of the polymer chain induced by the electrospinning process. The decrease of crystallite size as a function of the copolymer content is also observed. This suggests that the oxyethylene unit plays an important role in the orientation of the polymer chain. This result confirms our previous speculation that the stretching of the polymer chain during the electrospinning process is increased by the oxyethylene unit. Moreover, by increasing the copolymer content, the degree of crystallinity is decreased, which might result from the irregularity of the oxyethylene unit obstructing the packing structure of the polymer chain.

Thermal properties obtained from the DSC thermograms (not shown) also supported the above speculation. Both POM resin and electrospun POM shows that the higher the copolymer content, the lower the T_m (Table 4.2). However, crystallization temperatures of the electrospun POM is about 3–5°C higher than that of the POM resin. Enthalpy of melt generally reflects the degree of crystallinity of the polymer. In our case, the enthalpy of melt observed in the first heating (ΔH_m, 1st heating) implies the degree of crystallinity initiated by the electrospinning process. On the other hand, the enthalpy of melt observed in the second heating (ΔH_m, 2nd heating) implies the degree of crystallinity of the polymer after slowly cooling from the melt. For electrospun POM, the ΔH_m observed in the 1st heating is significantly higher than that observed in the 2nd heating, suggesting that the polymer chain alignment is induced by the electrospinning process. The result is relevant to the higher degree of crystallinity observed by the X-ray.

Specific surface area. The spinning conditions were varied to identify the reasons behind the inevitable porous appearance of the electrospun nanofibers. As

mentioned above, HFIP is a good solvent for POM electrospinning, where rapid evaporation based on the high vapor pressure might be the main factor inducing the regular nanopores. Here, a quantitative analysis to evaluate the fiber porosity was carried out using BET. Table 4.1 also shows the specific surface area values and pore specific volumes of the electrospun POM nanofibers with different fiber diameters. The specific surface areas are in the range of 15–57 m^2/g, depending on the fiber diameter and the significant porosity of the fibers. The highest specific surface area is observed for POM4.4/HFIP (~57 m^2/g) with a specific pore volume of 0.15 cm^3/g. Though the fiber diameter of POM13/HFIP is the smallest (~450 nm) as compared to the others, the specific surface area is only 15 m^2/g. This is due to less surface roughness and less porosity, compared to the others. Compared with other polymers—e.g. non-porous fiber, Nylon 6/formic acid (14–33 m^2/g)[29], and porous fiber, PAN (9.5 m^2/g)[30]—the POM nanofibers show significantly higher specific surface areas, which might lead to various potential applications in the future.

4. Conclusion

An electrospun polyoxymethylene (POM) nanofiber using a hexafluoroisopropanol (HFIP)-based solvent was successfully prepared by controlling the spinning conditions (i.e. electrostatic field strength and relative humidity) as well as the polymer/solvent properties (i.e. copolymer content and vapor pressure of the solvent). Nanopore formation was inevitable and was mainly induced via TIPS and VIPS mechanisms. A decrease in nanoporosity could be achieved under (i) an increase of the oxyethylene unit in the POM copolymer, (ii) a decrease of solvent vapor pressure, (iii) an increase of spinning voltage, and (iv) a decrease of relative humidity. Although electrospinning might induce the partial degradation of the POM, the nanofibers obtained showed a tensile strength as high as five times the bulk POM. Because the electrospun POM nanofibers have a nanoporous structure with a higher specific surface

area than Nylon6/formic acid or PAN, this information is a useful guideline for developing unique products such as nanoporous filters and membranes.

Acknowledgements. The authors are grateful for the financial support from Mitsubishi Gas Chemical Company, Japan, and Thai Polyacetal Co. Ltd., Thailand. The authors are appreciative of the grant from the University Mobility in Asia and the Pacific (UMAP) Program under the MOE, Thailand. One of the authors (T.K.) gratefully acknowledges the scholarship from the Petroleum and Petrochemical College, Chulalongkorn University.

Supporting Information Available: SEM images of POM0, POM1.5, and POM4.4 electrospun at different concentrations, SEM images of POM4.4 electrospun at various electrical voltages, and mechanical properties of aligned POM0 nanofibers. This information is available free of charge via the internet at http://pubs.acs.org.

References

(1) Samon, J.M.; Schultz, J.M.; Hsiao, B.S.; Khot, S.; Johnson, H.R. *Polymer* **2001**, 42, 1547–1559.

(2) Duan, Y.; Li, H.; Ye, L.; Liu, X. *Journal of Applied Polymer Science* **2006**, 99, 3085–3092.

(3) Reneker, D.H.; Chun, I. *Nanotechnology* **1996**, 7, 216–223.

(4) Berghoef, M.M.; Vansco, G.J. *Advanced Materials* **1999**, 11, 1362–1365.

(5) Bognitzki, M.; Czado. W.; Frese, T.; Schaper, A.; Hellweg, M.; Steinhart, M.; Greiner, A.; Wendorff, J.H. *Advanced Materials* **2001**, 13, 70–72.

(6) Doshi, J.; Reneker, D.H. *Journal of Electrostatic* **1995**, 35, 151–160.

(7) Givens, S.R.; Gardner, K.H.; Rabolt, J.F.; Chase, D.B. *Macromolecules* **2007**, 40, 608–610.

(8) Megelski, S.; Stephens, J.S.; Chase, D.B.; Rabolt, J.F. *Macromolecules* **2002**, 35, 8456–8466.

(9) Casper, C.L.; Stephens, J.S.; Tassi, N.G.; Chase, D.B.; Rabolt, J.F. *Macromolecules* **2004**, 37, 573–578.

(10) Zeng, J.; Aigner, A.; Czubayko, F.; Kissel, T.; Wendorff, J.H.; Greiner, A. *Biomacromolecules* **2005**, 6, 1484–1488.

(11) Yang, F.; Murugan, R.; Wang, S.; Ramakrishna, S. *Biomaterials* **2005**, 26, 2603–2610.

(12) Chen, J.P.; Chang, G.Y.; Chen, J.K. *Colloids and Surfaces A: Physicochem. Eng. Aspects* **2008**, 313–314, 183–188.

(13) Gibson, P.W.; Shreuder-Gibson, H.L.; Rivin, D. *AICHE Journal* **1999**, 45, 190–195.

(14) Gibson, P.W.; Shreuder-Gibson, H.L. *US Army Soldier and Biological Chemical Command Technical Report Natick/TR-99/016L* **1999**.

(15) Katarzyna, M.; Sawicka. P.G. *Journal of Nanoparticle Research* **2006**, 8, 769–771.

(16) Wang, X.; Drew, C.; Lee, S.H.; Senecal, K.J.; Kumar, J.; Samuelson, L.A. *Nano Letters* **2002**, 2, 1273–1275.

(17) Wang, A.; Singh, H.; Hatton, T.A.; Rutledge, G.C. *Polymer* **2004**, 45, 5505–5514.

(18) Iguchi, M. *Makromolekulare Chemie* **1976**, 177, 549–566.

(19) Deitzel, J.M.; Kleinmeyer, J.; Harris, D.; Beck Tan, N.C. *Polymer* **2001**, 42, 261–272.

(20) Koski, A.; Yim, K.; Shivkumar, S. *Materials Letters* **2004**, 58, 493–497.

(21) Demir, M.M.; Yilgor, I.; Yilgor, E.; Erman, B. *Polymer* **2002**, 43, 3303–3309.

(22) Gao, K.; Hu, X.; Dai, C.; Yi, T. *Materials Science and Engineering B* **2006**, 131, 100–105.

(23) Srinivasarao, M.; Collings, D.; Philips, A.; Patel, S. *Science* **2001**, 292, 79–83.

(24) Van de Witte, P.; Dijkstra, P.J.; van den Berg, J.W.A.; Feijen, J. *Journal of Membrane Science* **1996**, 117, 1–31.

(25) Park, H.C.; Kim, Y.P.; Kim, H.Y.; Kang, Y.S. *Journal of Membrane Science* **1999**, 156, 169–178.

(26) Liu, Y.; Cui, L.; Guan, F.; Gao, Y.; Hedin, N.E.; Zhu, L.; Fong, H. *Macromolecules* **2007**, 40, 6283–6290.

(27) Stephens, J.S.; Chase, D.B.; Rabolt, J.F. *Macromolecules* **2004**, 37, 877–881.

(28) Kongkhlang, T.; Tashiro, K.; Kotaki, M.; Kousaka, Y.; Umemura, T.; Nakaya, D.; Chirachanchai, S. *In preparation.*

(29) Ryu, Y.J.; Kim, H.Y.; Lee, K.H.; Park, H.C.; Lee, D.R. *European Polymer Journal* **2003**, 39, 1883–1889.

(30) McCann, J.T.; Marquez, M.; Xia, Y. *Journal of American Chemical Society* **2006**, 128, 1436–1437.